RESEARCH ARTICLE
SOLID EARTH: GEOMAGNETISM

Earth and Planetary Physics
7: 49–56, 2023
doi: 10.26464/epp2023011

A global mantle conductivity model derived from 8 years of Swarm satellite magnetic data

HongBo Yao[1,3], ZhengYong Ren[1,2,3*], KeJia Pan[4], JingTian Tang[1,2,3], and KeKe Zhang[5]

[1]Key Laboratory of Metallogenic Prediction of Nonferrous Metals and Geological Environment Monitoring, Ministry of Education (Central South University), Changsha 410083, China;

[2]Hunan Key Laboratory of Nonferrous Resources and Geological Hazards Exploration, Central South University, Changsha 410083, China;

[3]School of Geosciences and Info-Physics, Central South University, Changsha 410083, China;

[4]School of Mathematics and Statistics, Central South University, Changsha 410083, China;

[5]State Key Laboratory of Lunar and Planetary Sciences, Macau University of Science and Technology, Taipa, Macau, China

Key Points:

- A data processing and one-dimensional (1D) inversion scheme is developed for satellite induction magnetic data.
- This scheme is ready to process the forthcoming Macau ScienceSatellite-1 data.
- A new global mantle conductivity model is obtained by analyzing over 8 years of Swarm satellite data.

Citation: Yao, H. B., Ren, Z. Y., Pan, K. J., Tang, J. T., and Zhang, K. K. (2023). A global mantle conductivity model derived from 8 years of Swarm satellite magnetic data. *Earth Planet. Phys.*, *7*(1), 49–56. http://doi.org/10.26464/epp2023011

Abstract: Mantle conductivity imaging is one of the scientific goals of the forthcoming Macau Science Satellite-1 (MSS-1). To achieve this goal, we develop a data analysis and inversion scheme for satellite magnetic data to probe global one-dimensional (1D) mantle conductivity structures. Using this scheme,we present a new global mantle conductivity model by analyzing over 8 years of Swarm satellite magnetic data. First, after sophisticated data selection procedures and the removal of core and crustal fields, the inducing and induced spherical harmonic coefficients of magnetic potential due to the magnetospheric ring current are derived. Second, satellite *C*-responses are estimated from the time series of these coefficients. Finally, the observed responses are inverted for both smooth and three-jump conductivity models using a quasi-Newton algorithm. The obtained conductivity models are in general agreement with previous global mantle conductivity models. A comparison of our conductivity model with the laboratory conductivity model suggests the mean state of the upper mantle and transition zone is relatively dry. This scheme can be used to process the forthcoming Macau Science Satellite-1 magnetic data.

Keywords: Macau Science Satellite-1; satellite magnetic data; mantle conductivity; global electromagnetic induction

1. Introduction

At the beginning of 2023, the government of Macau Special Administrative Region and the China National Space Administration will jointly launch a low-latitude and low-inclination geomagnetic satellite, the Macau Science Satellite-1 (MSS-1), which will provide an accurate East–West gradient of the magnetic field. Imaging mantle electrical conductivity structures using the induction magnetic field is one of its scientific goals. However, satellite-measured magnetic fields consist of contributions from the core and crust, the magnetospheric and ionospheric current systems, as well as their induced counterparts (Olsen and Stolle, 2012), and the moving ocean induced magnetic field (Grayver et al., 2016; Zhang H et al., 2019). Consequently, this study concentrates on the development of a sophisticated data processing and inversion scheme and the compilation of a new global reference conductivity model using Swarm satellite magnetic data.

Electrical conductivity is sensitive to temperature variations and the presence of melt, and strongly depends on the water content and distribution in the Earth's mantle (Yoshino, 2010; Karato, 2011). By constraining mantle conductivity structures, we can further study the composition, structure, and dynamics of Earth's mantle. Natural geomagnetic variations with periods from several days to several months originating from external magnetospheric current systems can be used for mantle conductivity imaging (Kuvshinov, 2012). One main data source is the geomagnetic fields recorded by ground geomagnetic observatories (Olsen, 1998, 1999b; Shimizu et al., 2010; Xu GJ et al., 2015; Munch et al., 2018; Chen CJ et al., 2020; Yuan YR et al., 2020; Zhang YH et al., 2020; Zhang HQ et al., 2022). However, due to the sparse and irregular distribution, geomagnetic observatory data only has local scale resolution and lacks global scale resolution. Compared to geomagnetic observatory data, satellite data can provide full

Correspondence to: Z. Y. Ren, renzhengyong@csu.edu.cn
Received 11 APR 2022; Accepted 24 OCT 2022.
Accepted article online 23 NOV 2022.

coverage above the Earth's surface. These data are suitable for obtaining a global reference conductivity model, which is essential for understanding the mean physicochemical state of Earth's mantle.

Currently, several global 1D conductivity models have been derived from satellite magnetic measurements such as Magsat, CHAMP, Ørsted, and SAC-C (Olsen, 1999a; Constable and Constable, 2004; Kuvshinov and Olsen, 2006; Velímský et al., 2006; Velímský, 2010). Most studies only used the data measured by a single satellite, which may have a lot of data gaps. The latest Swarm satellite constellation (Olsen et al., 2013) as launched on November 22, 2013, consists of three identical satellites. With simultaneous observations of three satellites, the data gaps may be significantly reduced. Using Swarm data, several new global 1D conductivity models were proposed (Civet et al., 2015, Püthe, 2015; Grayver et al., 2017). But, the use of a relatively short time series of data (3 years or less than 1 year) can lead to scattered geomagnetic responses and noisy results (Kuvshinov and Olsec, 2006). Even in the latest mantle conductivity studies, only 6 years of Swarm satellite data were analyzed (Kuvshinov et al., 2021; Verhoeven, Thébault et al., 2021).

In this study, we develop a data analysis and inversion scheme for satellite magnetic data and present a new global reference conductivity model using more than 8 years of Swarm satellite constellation data. The structure of this manuscript is as follows. Section 2 describes the data processing and inversion scheme. In Section 3, we compare our conductivity model with previous global mantle conductivity models. We also discuss the mean physicochemical state of Earth's mantle by comparing our model with laboratory conductivity data. Finally, we present the conclusions and outlook for future studies.

2. Data and Method

2.1 Data Processing

The Swarm satellite constellation consists of three satellites (Swarm A, B, and C). We collected over 8 years of Swarm Level 1b vector magnetic data from 26/11/2013 to 31/12/2021. The measured magnetic fields consist of contributions from the core and crust, the magnetospheric and ionospheric current systems, as well as their induced counterparts (Olsen and Stolle, 2012), and the moving ocean induced magnetic field (Grayver et al., 2016; Zhang H et al., 2019). Before analyzing the induced data from the magnetospheric ring current, it is necessary to remove the non-induced parts to avoid misinterpretation (Olsen, 1999a). The raw data are processed as follows (see also Figure 1).

Step (1): Data selection. We keep only the vector magnetic data in nominal mode as identified by the quality flags defined in Swarm Level 1b Product Definition. To reduce the influences of ionospheric current systems such as the auroral electrojet and Sq current, we only use non-polar data at geomagnetic colatitude 40–140 degrees and night-side data at magnetic local time 19:00–05:00.

Step (2): Remove core and crustal fields from the original time series as predicted by the latest CHAOS-7 geomagnetic field model (Finlay et al., 2020).

Step (3): Rotate the horizontal field components from geographic to geomagnetic coordinate systems using the geomagnetic north pole of IGRF 2015 (International Geomagnetic Reference Field 2015) model. Delete outliers according to three standard deviations.

After these procedures, the residual field is assumed to only contain the contributions from the large-scale magnetospheric current systems and their induced counterparts, which can reach hundreds of nT. The moving ocean induced magnetic field, which is only 1–2 nT at satellite altitudes, is ignored due to its small amplitude. The residual magnetic field $\boldsymbol{B}$ can be represented by the gradient of a magnetic scalar potential V, that is $\boldsymbol{B} = -\nabla V$. For periods from several days to several months, the residual magnetic field is related to the magnetospheric ring current which may be approximated by the first zonal spherical harmonic $Y_1^0 = \cos\theta$ (Banks and Ainsworth, 1992) with θ being the geomagnetic colatitude. The magnetic scalar potential reads

$$V(r,\theta,t) = a\left[\varepsilon_1^0(t)\left(\frac{r}{a}\right) + \iota_1^0(t)\left(\frac{a}{r}\right)^2\right]\cos\theta, \tag{1}$$

where a = 6371.2 km is Earth's mean radius, r is the radial distance from the Earth's center, t denotes the time dependence of the magnetic potential, ε_1^0 and ι_1^0 are the inducing (external) and induced (internal) spherical harmonic coefficients. Therefore, the corresponding magnetic field can be written as

$$B_r(r,\theta,t) = \left[-\varepsilon_1^0(t) + 2\iota_1^0(t)\left(\frac{a}{r}\right)^3\right]\cos\theta, \tag{2}$$

$$B_\theta(r,\theta,t) = \left[\varepsilon_1^0(t) + \iota_1^0(t)\left(\frac{a}{r}\right)^3\right]\sin\theta, \tag{3}$$

$$B_\varphi(r,\theta,t) = 0, \tag{4}$$

with B_r, B_θ, B_φ being the radial, colatitude, and longitudinal components of the magnetic field.

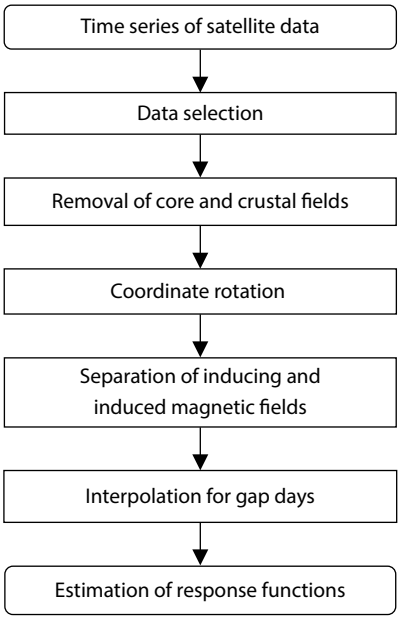

Figure 1. Flowchart of satellite data processing.

Step (4): Separation of inducing and induced magnetic fields. The residual field is used to fit Equations (2) and (3) on a daily basis by iteratively reweighted least squares method (Aster et al., 2018), then the time series of inducing $\varepsilon_1^0(t)$ and induced $\iota_1^0(t)$ coefficients can be obtained.

Step (5): Interpolation for gap days. For a total of 2,958 days from 26/11/2013 to 31/12/2021, if only using a single satellite data, the numbers of gap days for Swarm A, B, and C are 399, 416, and 2,658, respectively. The large gaps for Swarm C are due to the fact that the data after 5/11/2014 are not in nominal mode, as also noted in Verhoeven et al. (2021). If using all three satellite data, the number of gap days is only 70. Therefore, using satellite constellation data has significantly reduced the gaps in the data. The inducing and induced coefficients of these 70 days are interpolated using the *Dst* index, as done by Civet et al. (2015). Figure 2a shows the final time series of inducing and induced spherical harmonic coefficients. Our results show that the induced coefficients ι_1^0 are smaller than the inducing coefficients ε_1^0. This result is in agreement with the fact that the induced coefficients are generated by the inducing coefficients. Similar results are also obtained by recent satellite electromagnetic induction studies (Kuvshinov et al., 2021; Verhoeven et al., 2021).

Step (6): Fourier transform. The time series of inducing $\varepsilon_1^0(t)$ and induced $\iota_1^0(t)$ coefficients are transformed to frequency domain values of $\varepsilon_1^0(\omega)$ and $\iota_1^0(\omega)$ by Fourier transform (Figure 2b), where $\omega = 2\pi/T$ is the angular frequency with T being the period. The shortest period is 2 days since we fit the time series on a daily basis.

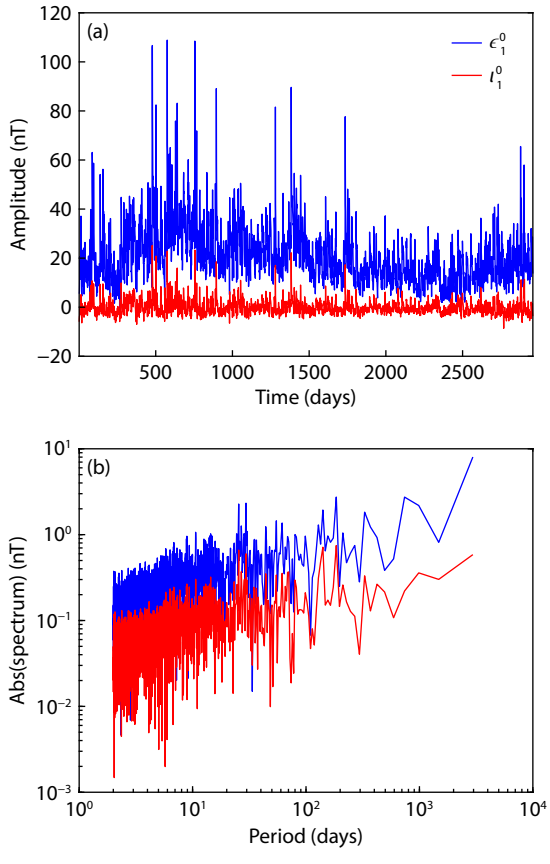

Figure 2. (a) Time series of inducing ε_1^0 and induced ι_1^0 coefficients estimated from over 8 years of Swarm vector magnetic data. The *x*-axis starts from November 26, 2013. (b) The corresponding Fourier spectrum.

Step (7): Estimation of geomagnetic response functions. Under the Y_1^0 source and 1D conductivity model assumptions, we estimate the scalar *Q*-responses in frequency domain (Olsen, 1999a) using the section-averaging approach (Semenov and Kuvshinov, 2012) and the iteratively reweighted least-square method (Aster et al., 2018). The data uncertainty $\delta Q(\omega)$ is estimated by the jackknife approach (Chave and Thomson, 1989). Then the scalar *Q*-responses are converted to the widely used *C*-responses (Kuvshinov and Olsen, 2006)

$$C(\omega) = \frac{a}{2}\frac{1-2Q(\omega)}{1+Q(\omega)}, \tag{5}$$

$$\delta C(\omega) = \frac{3a}{2}\frac{1}{\left|1+Q(\omega)\right|^2}\delta Q(\omega), \tag{6}$$

where $\delta C(\omega)$ is the uncertainty of the estimated *C*-responses.

2.2 Inversion for Mantle Conductivity Model

We aim at obtaining a globally averaged 1D conductivity model. In this case, the Earth's conductivity is assumed to only vary with depth. The conductivity model from Earth's surface to the core-mantle boundary is discretized into N_m discrete layers. The starting layer has a thickness of 10 km. The thicknesses of underlying layers increase gradually with depth by a step size of 1.1. A high conductivity value of 1×10^5 S/m is set for the Earth's core. We define the model vector $\boldsymbol{m} = [m_1, m_2, \cdots, m_{N_m}]$ as the logarithmic conductivity, that is $m_i = \log(\sigma_i), i = 1, 2, \cdots, N_m$ with σ_i being the conductivity of the i-layer. Logarithmic parametrization is used to guarantee the positiveness of conductivity values.

We seek the inverse models by minimizing the misfit between observed data and model predictions with additional constraints

$$\phi(\boldsymbol{m},\lambda) = \sum_{j=1}^{N_d}\frac{\left|C^{\rm obs}(\omega_j)-C^{\rm pred}(\boldsymbol{m},\omega_j)\right|^2}{\left[\delta C^{\rm obs}(\omega_j)\right]^2} + \lambda\sum_{i=2}^{N_m}s_i(m_i-m_{i-1})^2, \tag{7}$$

where N_d is the total number of observed data, $C^{\rm obs}(\omega_j)$ is observed *C*-response at an angular frequency of ω_j with $\delta C^{\rm obs}(\omega_j)$ being the data uncertainty. $C^{\rm pred}(\boldsymbol{m},\omega_j)$ is the predicted *C*-response, which is computed analytically using the recursive formulation of Kuvshinov and Semenov (2012) for a given 1D model $\boldsymbol{m}$. The s_i is a factor that controls the smoothness between adjacent layers at the i-th interface. Unless otherwise stated, a value of 1.0 is adopted in this study, which is consistent with recent inversions of satellite magnetic data (Civet et al., 2015; Verhoeven et al., 2021). Using smaller values allows us to generate conductivity models with distinct jumps. The λ is the regularization parameter used to balance the data misfit and the smoothness of conductivity models. In our implementation, a set of independent inversions are performed with a fixed value of λ, the optimal λ is determined by *L*-curve analysis (Hansen, 1992).

The inverse problem is solved by the Limited-memory Broyden-

Fletcher-Goldfarb-Shanno (L-BFGS) optimization algorithm (Nocedal and Wright, 2006). The initial model is set to a uniform conductivity of 1 S/m. Then the model parameters are iteratively updated, and the inversion is terminated once one of the following conditions is reached. (1) The number of iterations reaches 100; (2) The root mean square (RMS) data misfit is just ≤ 1.0; (3) The RMS difference between adjacent iterations is less than 10^{-4}.

To validate the correctness of our inversion scheme, we invert the satellite *C*-responses estimated by Püthe et al. (2015). The results are shown in Figure 3. For comparison, the inverse model and the corresponding predicted responses of Püthe et al. (2015) are also shown. We observe an excellent agreement between our inversion results and those of Püthe et al. (2015), demonstrating the correctness of our inversion algorithm. The small differences are due to the different model regularizations.

3. Results and Discussion

3.1 Geomagnetic Responses

The observed satellite *C*-responses were estimated for a total of 20 equally logarithmic spaced periods from 3.04 to 81.37 days. In this period range, the geomagnetic variations are dominated by the magnetospheric ring current (Banks and Ainsworth, 1992). Shorter periods were discarded to further reduce the influences of the ionospheric current systems. Longer periods were not considered since the time series is too short. The final *C*-responses estimated using 2 years, 5 years, and over 8 years of satellite data are illustrated in Figure 4.

The responses estimated with longer time series of data show smaller uncertainties, indicating better data quality. This result demonstrates the advantage of using long time series of data. For comparison, the *C*-responses of Püthe et al. (2015) over the same period range are also shown. An overall good agreement is obtained, but the real parts of our data are slightly larger than those of Püthe et al. (2015) at short periods. This is most probably due to the use of different data sets. Püthe et al. (2015) used Oersted, CHAMP, SAC-C, and Swarm satellite data, as well as global geomagnetic observatory data. For the Swarm satellite, they used 8 months of data, while we used over 8 years of data.

3.2 Conductivity Models

The satellite *C*-responses estimated with 2, 5, and 8 years of data were inverted for mantle conductivity structures. For the responses estimated with 8 years of data, we also generated a three-jump conductivity model by setting the smooth factor to 0.1 at 410, 520, and 660 km depths. Figure 5 illustrates the final convergence curves of RMS misfit for all inversions. All inversions converge to similar RMS misfit values. The detailed RMS values for inversions of 2 years, 5 years, 8 years of data, and 8 years of data with a smooth factor of 0.1 are 1.54, 1.68, 1.79, and 1.67, respectively. The corresponding data fits are shown in Figure 6. The predicted responses fit the observed responses fairly well for the real parts. The imaginary parts of the observed responses are not fitted within uncertainties at short periods. This is likely related to the near-surface ocean effects which have not been considered in the present data processing procedure. One of our future works is to account for the ocean effects using a method similar to that of Püthe et al. (2015).

Figure 7 shows the corresponding inverse conductivity models. The results for inversions of 5 years and 8 years of data are similar. Below 1,200 km, these two models show an approximately constant conductivity value of ~1.8 S/m. However, the conductivity model obtained from only 2 years of data show distinct differences. Above 800 km, the conductivity model is more conductive. In the lowermost mantle, the model shows a constant value of about 1.2 S/m, which is close to the initial model. These differences can be attributed to the large uncertainties in the estimated responses as shown in Figure 4. These results demonstrate that using long time series of data is crucial for obtaining reliable conductivity structures.

Due to the use of smooth constraint and the diffusion nature of long-period electromagnetic fields, our smooth models show a monotonic increase in conductivity. The conductivity jumps at main mineral phase transition depths (410, 520, and 660 km) (Karato, 2011; Yoshino, 2010) are not shown. To allow jumps, we

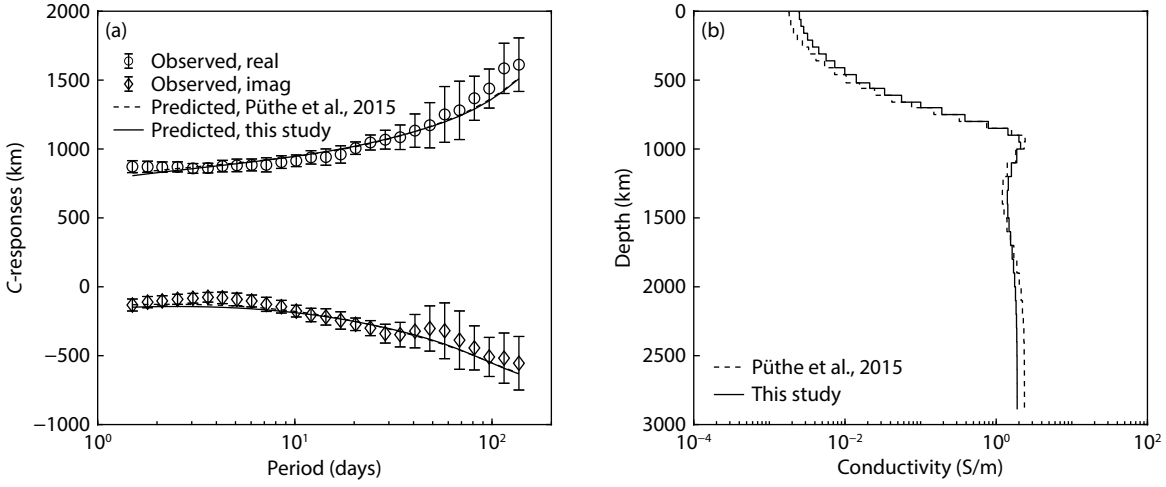

Figure 3. Validation of our inversion scheme. (a) Comparison of the observed (Püthe et al., 2015) and predicted *C*-responses computed for previous (Püthe et al., 2015) and our inverse models. (b) Comparison of our inverse model with the model obtained by Püthe et al. (2015).

released the smooth factors to 0.1 at these depths. The obtained three-jump conductivity model is also shown in Figure 7. We observe that when releasing the smooth constraint, the upper mantle and transition zone become more resistive, and distinct conductivity jumps are generated. However, the conductivity jumps are counterbalanced by the more conductive lower mantle over 660 and 1000 km depth range. This result may suggest that the conductivity jumps are consistent but not strictly required by the data. Therefore, we choose the smooth model derived from over 8 years of data as our preferred model.

For comparison, previous global 1D conductivity models (Civet et al., 2015; Püthe et al., 2015; Grayver et al., 2017; Kuvshinov et al., 2021) derived from satellite data are also shown in Figure 7. The

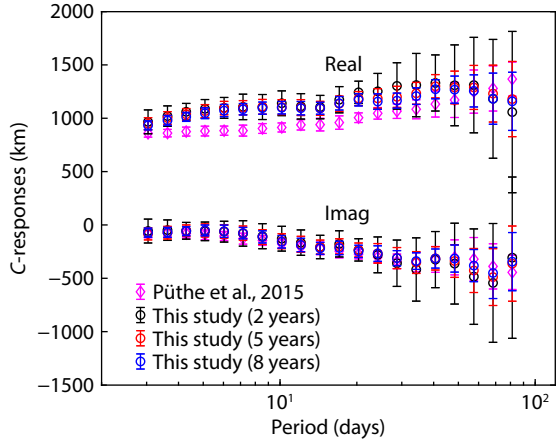

Figure 4. Comparison of our observed *C*-responses estimated from over 2, 5, and 8 years of Swarm satellite magnetic data with previous results (Püthe et al., 2015) estimated from over 10 years of satellite and observatory magnetic data. Error bars denote data uncertainties.

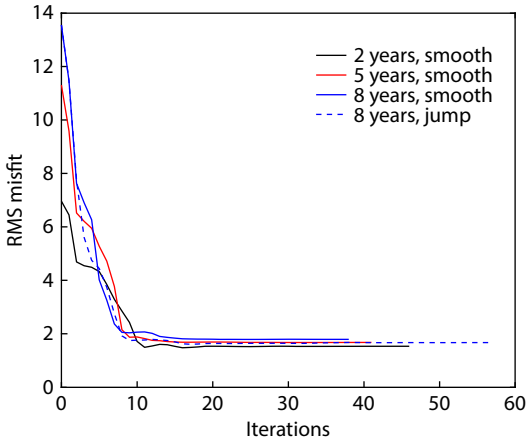

Figure 5. Convergence curves of RMS misfit for inversions of 2 years, 5 years, and 8 years of satellite data.

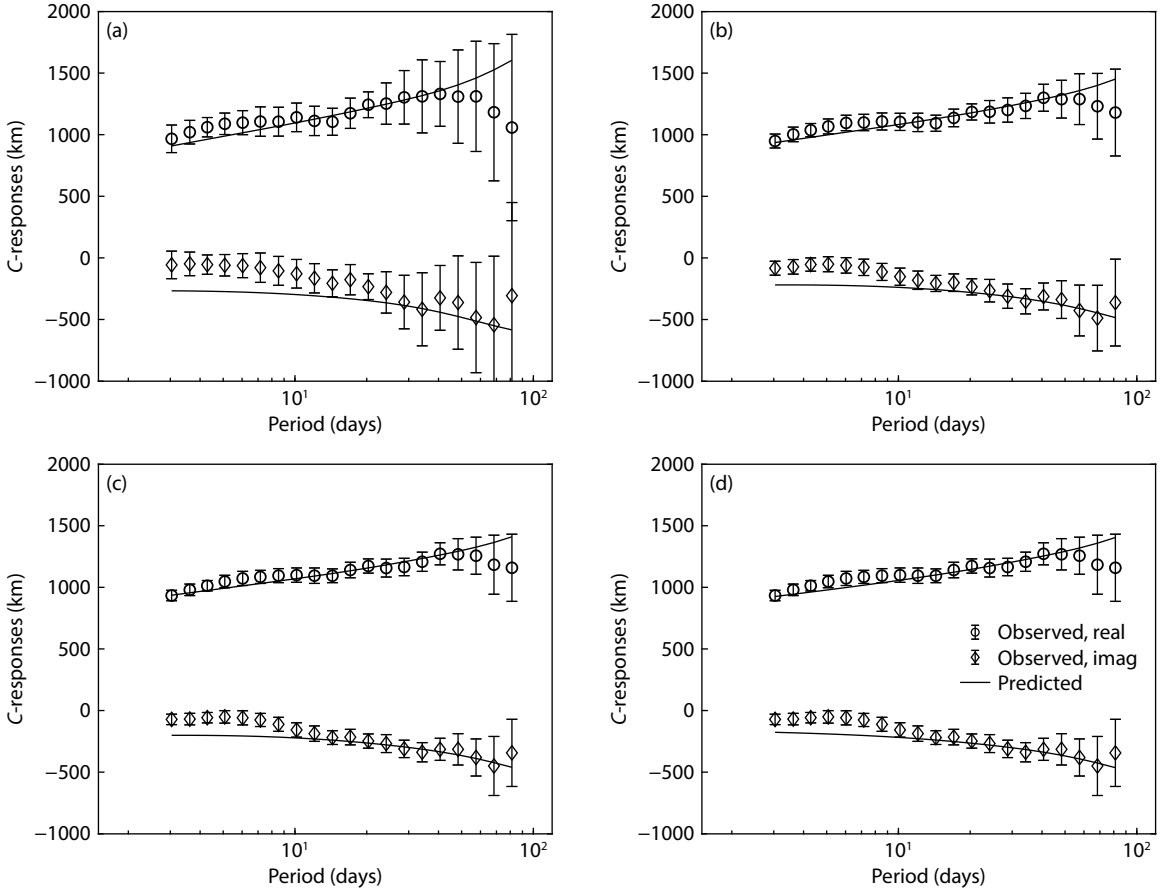

Figure 6. Comparison of observed (symbols) and predicted (lines) *C*-responses. Panels (a), (b), and (c) denote the inversions of 2 years, 5 years, and 8 years of satellite data. Panel (d) denotes the inversion of 8 years of satellite data while allowing jumps at 410, 520, and 660 km depths.

conductivity model of Püthe et al. (2015) was derived from over 10 years of satellite and observatory magnetic data by accounting for the near-surface ocean effects. An overall good agreement between our preferred model and the model of Püthe et al. (2015) is observed. However, our model is slightly more conductive in and above the mantle transition zone. Note that after correcting for the ocean effects, our model may become slightly more resistive in the upper mantle. We will discuss this issue in future work. The conductivity model of Civet et al. (2015) was derived from 10 months of Swarm satellite data. Compared to the model of Püthe et al. (2015) and our preferred model, their model shows a more sharp conductivity increase with depth. This may be caused by the use of relatively short data. The models of Grayver et al. (2017) and Kuvshinov et al. (2021) were derived by joint inversion of satellite magnetospheric and tidal magnetic signals. Compared to the magnetospheric magnetic signals used by Püthe et al. (2015), Civet et al. (2015) and this study, the tidal magnetic signals are more sensitive to the oceanic upper mantle (Grayver et al., 2016; Zhang H et al., 2019). This may interpret the large differences in and above the mantle transition zone.

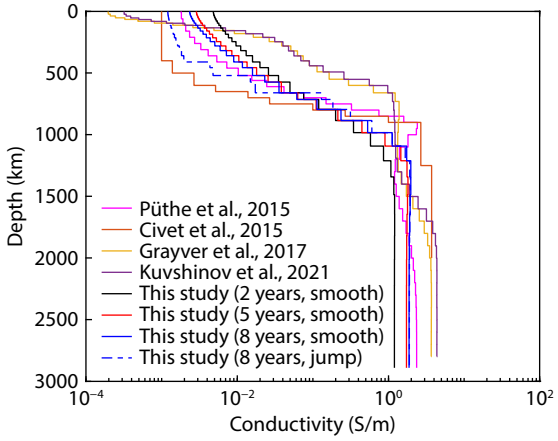

Figure 7. Comparison of our smooth and three-jump conductivity models obtained from over 2, 5, and 8 years of Swarm satellite magnetic data with previous global 1D mantle conductivity models (Civet et al., 2015; Püthe et al., 2015; Grayver et al., 2017; Kuvshinov et al., 2021).

3.3 Preliminary Discussion on Mantle Water Content

The electrical conductivity is sensitive to temperature variations and the water content of Earth's mantle. The conductivity of mantle minerals can be expressed with an Arrhenian relation, in which the conductivity value is a function of temperature and water content (Yoshino, 2010; Karato, 2011). Therefore, by comparing the geophysical inverse conductivity models with laboratory-measured conductivity data, we can constrain the water content of Earth's mantle.

The laboratory-measured conductivity data of Karato (2011) for main mantle minerals olivine (ol, upper mantle), wadsleyite (wad, upper mantle transition zone), and ringwoodite (ring, lower mantle transition zone) were considered. The latest adiabatic temperature model (Figure 8a) (Katsura, 2022) was adopted to construct the laboratory conductivity-depth profile.

The comparison of our preferred conductivity model with the laboratory conductivity–depth profile with fixed water content is shown in Figure 8b. Our preferred model is consistent with a dry upper mantle. In the mantle transition zone, our model is in good agreement with 0.001 wt% water content in the wadsleyite. These results suggest a relatively dry upper mantle and transition zone, in agreement with a recent mantle conductivity study (Zhang HQ et al., 2022).

4. Conclusions

We have developed a full data analysis and 1D inversion scheme for multiple satellite magnetic measurements. Our inversion scheme can generate both smooth conductivity models and models with sharp jumps. By analyzing more than 8 years of Swarm satellite magnetic data, we have clearly demonstrated that (1) using multiple satellite data simultaneously can significantly reduce the gaps in the data, and (2) using long time series of data

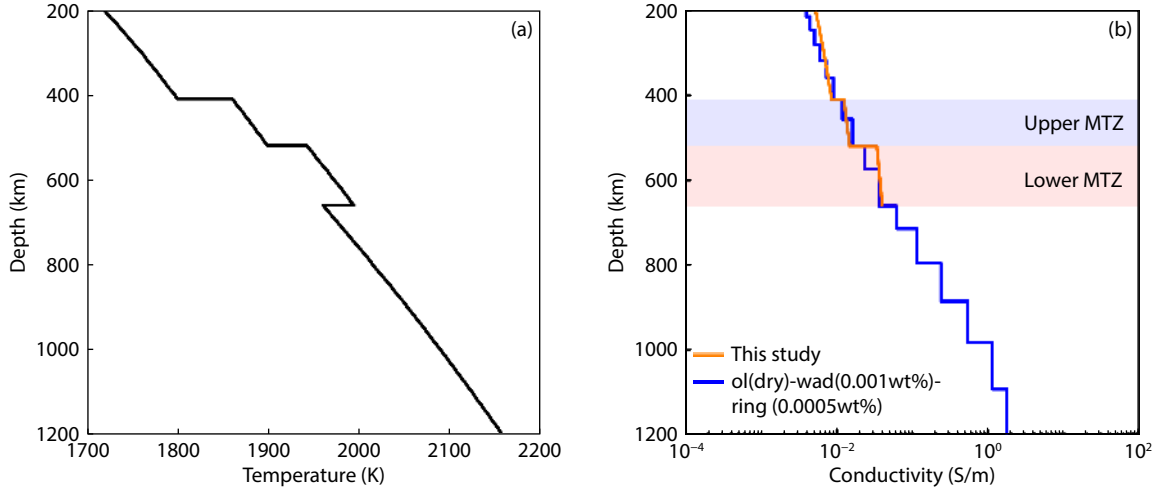

Figure 8. (a) The average mantle temperature profile of Katsura (2022) and (b) the comparison of our preferred inverse conductivity model with the laboratory conductivity model constructed using the data of Karato (2011). The shaded region denotes the upper and lower parts of the mantle transition zone (MTZ).

can reduce the data uncertainties and improve the results of geomagnetic responses and conductivity models.

Using this scheme, we obtained new global mantle conductivity models including a smooth conductivity model and a three-jump model that shows sharp jumps at main mineral phase transition depths. Although different in detail, our conductivity models are in good agreement with previous global average conductivity models derived from satellite magnetic data. By comparing with the laboratory-measured conductivity model, our model suggests that the global average mantle is relatively dry. Further improvements in laboratory high-pressure and high-temperature experiments are needed to reduce the uncertainty related to the laboratory conductivity data.

Future work should focus on the following aspects. First, to improve the reliability of upper mantle conductivity structures, correction for the ocean effects is crucial. Second, to improve the resolution of mantle conductivity models, we need to jointly invert multi-source geomagnetic responses. Finally, the accurate East–West gradient of the magnetic field as will be provided by the forthcoming MSS-1 will enhance our understanding of the non-axisymmetric magnetospheric current sources. Considering the induced magnetic field due to these current sources may further improve the reliability of inverse conductivity models.

Acknowledgments

This work was financially supported by the National Natural Science Foundation of China (41922027, 41830107, 42142034, 41874086), Innovation-Driven Project of Central South University (2020CX012), Macau Foundation and Macau Science and Technology Development Fund (0001/2019/A1), the Pre-research Project on Civil Aerospace Technologies funded by China National Space Administration (D020303), the Hunan Provincial Innovation Foundation for Postgraduate (CX20210277), and the Fundamental Research Funds for the Central Universities of Central South University (2021zzts0259). The valuable comments and suggestions by two anonymous reviewers have greatly improved the manuscript. We are grateful for resources from the High Performance Computing Center of Central South University. We thank the European Space Agency for providing access to Swarm magnetic data (https://earth.esa.int/eogateway/missions/swarm/data) and World Data Center for Geomagnetism, Kyoto for providing access to Dst index (http://wdc.kugi.kyoto-u.ac.jp/dstae/index.html). The satellite *C*-responses and conductivity models derived in this study are available at GitHub (https://github.com/hongbo-yao/MantleConductivityProfile).

References

Aster, R. C., Borchers, B., and Thurber, C. H. (2018). *Parameter Estimation and Inverse Problems*. Amsterdam, Netherlands: Elsevier.

Banks, R. J., and Ainsworth, J. N. (1992). Global induction and the spatial structure of mid-latitude geomagnetic variations. *Geophys. J. Int.*, *110*(2), 251–266. https://doi.org/10.1111/j.1365-246x.1992.tb00871.x

Chave, A. D., and Thomson, D. J. (1989). Some comments on magnetotelluric response function estimation. *J. Geophys. Res.*: *Solid Earth*, *94*(B10), 14215–14225. https://doi.org/10.1029/jb094ib10p14215

Chen, C. J., Kruglyakov, M., and Kuvshinov, A. (2020). A new method for accurate and efficient modeling of the local ocean induction effects. Application to long-period responses from island geomagnetic observatories. *Geophys. Res. Lett.*, *47*(8), e2019GL086351. https://doi.org/10.1029/2019gl086351

Civet, F., Thébault, E., Verhoeven, O., Langlais, B., and Saturnino, D. (2015). Electrical conductivity of the Earth's mantle from the first Swarm magnetic field measurements. *Geophys. Res. Lett.*, *42*(9), 3338–3346. https://doi.org/10.1002/2015gl063397

Constable, S., and Constable, C. (2004). Observing geomagnetic induction in magnetic satellite measurements and associated implications for mantle conductivity. *Geochem., Geophys., Geosyst.*, *5*(1), Q01006. https://doi.org/10.1029/2003gc000634

Finlay, C. C., Kloss, C., Olsen, N., Hammer, M. D., Tøffner-Clausen, L., Grayver, A., and Kuvshinov, A. (2016). The CHAOS-7 geomagnetic field model and observed changes in the South Atlantic Anomaly. *Earth, Planets Space*, *72*(1), 156. https://doi.org/10.1186/s40623-020-01252-9

Grayver, A. V., Schnepf, N. R., Kuvshinov, A. V., Sabaka, T. J., Manoj, C., and Olsen, N. (2016). Satellite tidal magnetic signals constrain oceanic lithosphere-asthenosphere boundary. *Sci. Adv.*, *2*(9). https://doi.org/10.1126/sciadv.1600798

Grayver, A. V., Munch, F. D., Kuvshinov, A. V., Khan, A., Sabaka, T. J., Tøffner-Clausen, L. (2017). Joint inversion of satellite-detected tidal and magnetospheric signals constrains electrical conductivity and water content of the upper mantle and transition zone. *Geophys. Res. Lett.*, *44*(12), 6074–6081. https://doi.org/10.1002/2017gl073446

Hansen, P. C. (1992). Analysis of discrete ill-posed problems by means of the L-curve. *SIAM Rev.*, *34*(4), 561–580. https://doi.org/10.1137/1034115

Karato, S. I. (2011). Water distribution across the mantle transition zone and its implications for global material circulation. *Earth Planet Sci. Lett.*, *301*(3-4), 413–423. https://doi.org/10.1016/j.epsl.2010.11.038

Katsura, T. (2022). A revised adiabatic temperature profile for the mantle. *J. Geophys. Res.*: *Solid Earth*, *127*(2), e2021JB023562. https://doi.org/10.1029/2021jb023562

Kuvshinov, A., and Olsen, N. (2006). A global model of mantle conductivity derived from 5 years of CHAMP, Ørsted, and SAC-C magnetic data. *Geophys. Res. Lett.*, *33*(18), L18301. https://doi.org/10.1029/2006gl027083

Kuvshinov, A. V. (2012). Deep electromagnetic studies from land, sea, and space: Progress status in the past 10 years. *Surv. Geophy.*, *33*(1), 169–209. https://doi.org/10.1007/s10712-011-9118-2

Kuvshinov, A., and Semenov, A. (2012). Global 3-D imaging of mantle electrical conductivity based on inversion of observatory *C*-responses-I. An approach and its verification. *Geophys. J. Int.*, *189*(3), 1335–1352. https://doi.org/10.1111/j.1365-246x.2011.05349.x

Kuvshinov, A., Grayver, A., Tøffner-Clausen, L., and Olsen, N. (2021). Probing 3-D electrical conductivity of the mantle using 6 years of Swarm, CryoSat-2 and observatory magnetic data and exploiting matrix Q-responses approach. *Earth, Planets Space*, *73*(1), 67. https://doi.org/10.1186/s40623-020-01341-9

Munch, F. D., Grayver, A. V., Kuvshinov, A., and Khan, A. (2018). Stochastic inversion of geomagnetic observatory data including rigorous treatment of the ocean induction effect with implications for transition zone water content and thermal structure. *J. Geophys. Res.*: *Solid Earth*, *123*(1), 31–51. https://doi.org/10.1002/2017jb014691

Nocedal, J., and Wright, S. J. (2006). *Numerical Optimization* (2nd ed). New York, NY: Springer.

Olsen, N. (1998). The electrical conductivity of the mantle beneath Europe derived from *C*-responses from 3 to 720 hr. *Geophys. J. Int.*, *133*(2), 298–308. https://doi.org/10.1046/j.1365-246x.1998.00503.x

Olsen, N. (1999a). Induction studies with satellite data. *Surv. Geophys.*, *20*(3-4), 309–340. https://doi.org/10.1023/a:1006611303582

Olsen, N. (1999b). Long-period (30 days-1 year) electromagnetic sounding and the electrical conductivity of the Lower Mantle Beneath Europe. *Geophys. J. Int.*, *138*(1), 179–187. https://doi.org/10.1046/j.1365-246x.1999.00854.x

Olsen, N., and Stolle, C. (2012). Satellite geomagnetism. *Ann. Rev. Earth Planet. Sci.*, *40*(1), 441–465. https://doi.org/10.1146/annurev-earth-042711-105540

Olsen, N., Friis-Christensen, E., Floberghagen, R., Alken, P., Beggan, C. D., Chulliat, A., Doornbos, E., Da Encarnação, J. T., Hamilton, B., ... Visser, P. N. (2013). The *Swarm* satellite constellation application and research facility (SCARF) and *Swarm* data products. *Earth, Planets Space*, *65*(11), 1189–1200.

https://doi.org/10.5047/eps.2013.07.001

Püthe, C., Kuvshinov, A., Khan, A., and Olsen, N. (2015). A new model of Earth's radial conductivity structure derived from over 10 yr of satellite and observatory magnetic data. *Geophys. J. Int.*, *203*(3), 1864–1872. https://doi.org/10.1093/gji/ggv407

Semenov, A., and Kuvshinov, A. (2012). Global 3-D imaging of mantle conductivity based on inversion of observatory *C*-responses-II. Data analysis and results. *Geophys. J. Int.*, *191*(3), 965–992. https://doi.org/10.1111/j.1365-246x.2012.05665.x

Shimizu, H., Koyama, T., Baba, K., and Utada, H. (2010). Revised 1-D mantle electrical conductivity structure beneath the North Pacific. *Geophys. J. Int.*, *180*(3), 1030–1048. https://doi.org/10.1111/j.1365-246x.2009.04466.x

Velímský, J., Martinec, Z., and Everett, M. E. (2006). Electrical conductivity in the Earth's mantle inferred from CHAMP satellite measurements-I. Data processing and 1-D inversion. *Geophys. J. Int.*, *166*(2), 529–542. https://doi.org/10.1111/j.1365-246x.2006.03013.x

Velímský, J. (2010). Electrical conductivity in the lower mantle: Constraints from CHAMP satellite data by time-domain EM induction modelling. *Phys. Earth Planet. Interiors*, *180*(3-4), 111–117. https://doi.org/10.1016/j.pepi.2010.02.007

Verhoeven, O., Thébault, E., Saturnino, D., Houliez, A., and Langlais, B. (2021). Electrical conductivity and temperature of the Earth's mantle inferred from Bayesian inversion of Swarm vector magnetic data. *Phys. Earth Planet. Interiors*, *314*, 106702. https://doi.org/10.1016/j.pepi.2021.106702

Xu, G. J., Tang, J., Huang, Q. H., and Uyeshima, M. (2015). Study on the conductivity structure of the upper mantle and transition zone beneath North China. *Chin. J. Geophys.* (*in Chinese*), *58*(2), 566–575. https://doi.org/10.6038/cjg20150219

Yoshino, T. (2010). Laboratory electrical conductivity measurement of mantle minerals. *Surv. Geophys.*, *31*(2), 163–206. https://doi.org/10.1007/s10712-009-9084-0

Yuan, Y. R., Uyeshima, M., Huang, Q. H., Tang, J., Li, Q., and Teng, Y. T. (2020). Continental-scale deep electrical resistivity structure beneath china. *Tectonophysics*, *790*, 228559. https://doi.org/10.1016/j.tecto.2020.228559

Zhang, H., Egbert, G. D., Chave, A. D., Huang, Q., Kelbert, A., and Erofeeva, S. Y. (2019). Constraints on the resistivity of the oceanic lithosphere and asthenosphere from seafloor ocean tidal electromagnetic measurements. *Geophys. J. Int.*, *219*(1), 464–478. https://doi.org/10.1093/gji/ggz315

Zhang, H. Q., Egbert, G. D., and Huang, Q. H. (2022). A relatively dry mantle transition zone revealed by geomagnetic diurnal variations. *Sci. Adv.*, *8*(31), eabo3293. https://doi.org/10.1126/sciadv.abo3293

Zhang, Y. H., Weng, A. H., Li, S. W., Yang, Y., Tang, Y., and Liu, Y. H. (2020). Electrical conductivity in the mantle transition zone beneath Eastern China derived from L_1-Norm *C*-responses. *Geophys. J. Int.*, *221*(2), 1110–1124. https://doi.org/10.1093/gji/ggaa059